Article

Biological Efficacy Comparison of Natural Tussah Silk and Mulberry Silk Nanofiber Membranes for Guided Bone Regeneration

Yumao Chen,[¶] Ming Chen,[¶] Yang Gao, Feng Zhang, Min Jin, Shijun Lu,* and Minxuan Han*

Cite This: *ACS Omega* 2022, 7, 19979−19987

Read Online

ACCESS | Metrics & More | Article Recommendations

ABSTRACT: Biopolymer nanofiber membranes are attracting interest as promising biomaterial scaffolds with a remarkable range of structural and functional performances for guided bone regeneration (GBR). In this study, tussah silk nanofiber (TSn) and *Bombyx mori* silk nanofiber (BSn) membranes were prepared by physical shearing. The diameters of the TSn and BSn membranes were 146.09 ± 63.56 and 120.99 ± 91.32 nm, respectively. TSn showed a Young's modulus of 3.61 ± 0.64 GPa and a tensile strength of 74.27 ± 5.19 MPa, which were superior to those of BSn, with a Young's modulus of 0.16 ± 0.03 GPa and a tensile strength of 4.86 ± 0.61 MPa. The potential of TSn and BSn membranes to guide bone regeneration was explored. In vitro, the TSn membrane exhibited significantly higher cell proliferation for MC3T3-E1 cells than the BSn membrane. In a cranial bone defect

in a rat model, the TSn and BSn membranes displayed superior bone regeneration compared to the control because the membrane prevented the ingrowth of soft tissue to the defective area. Compared to the BSn membrane, the TSn membrane improved damaged bone regeneration, presumably due to its superior mechanical properties, high osteoconductivity, and increased cell proliferation. The TSn membrane has a bionic structure, excellent mechanical properties, and greater biocompatibility, making it an ideal candidate for GBR.
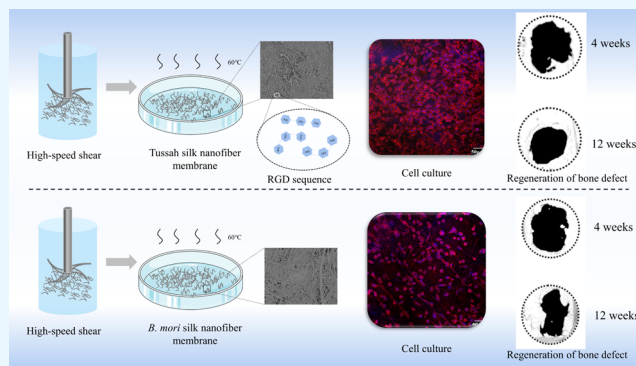
1. INTRODUCTION

Guided bone regeneration (GBR) is a procedure aiming for the reconstruction of impaired bone tissue. The GBR technique makes use of a membrane that is used in the interface between soft tissue and restoration areas, aiming to resist the migration of faster-growing connective tissue into the bone defect. Meanwhile, the membrane provides a protected space for bone defects, thus allowing the migration of osteoblasts and the ingrowth of a new bone.[1,2] The membrane is a critical component of the GBR technique for successful bone regeneration. The ideal GBR membrane should have several desirable properties, including biocompatibility, structural and mechanical stability, tissue integration, and proper degradation rate.[3,4] Therefore, many studies have been conducted on GBR membranes from various natural and synthetic sources to meet clinical needs.[5]

Generally, two types of GBR membranes (resorbable and nonresorbable) have been used in terms of their degradation characteristics.[6] Nonresorbable membranes, mainly titanium mesh and polytetrafluoroethylene, exhibit high biocompatibility, mechanical properties, and stability.[7] However, the lack of biodegradability requires a secondary surgical procedure for removal,[8] which may cause soft tissue dehiscence, resulting in the likelihood of wound infection and an extended healing period. Thereafter, the resorbable membrane, aiming to obviate the need for additional surgery, has been developed and widely used in clinical practice. These membranes are usually made of natural or synthetic polymers, such as polyglycolic acid, polylactic acid, polycaprolactone, and their copolymers or collagen.[9] As the representative resorbable GBR membrane, collagen shows excellent biocompatibility and positive results in clinical use. However, collagen still have several disadvantages, including antigenicity, rapid degradation, and low stiffness.[8] Many studies are being conducted to develop new membranes for GBR.

Silk fibroin (SF), secreted by silkworms, is a representative biomaterial.[10] Recently, SF has gained increasing attention for potential application as a GBR membrane because of several characteristics, including good biocompatibility, controllable degradation, remarkable mechanical properties, and less

foreign body reaction.[10−12] Compared to *Bombyx mori* silk, tussah silk is a more promising candidate for GBR due to its natural arginine−lysine−aspartate (RGD) known as a cell adhesion sequence.[13] It has been found that tussah silk exhibits osteoconductivity superior to that of *B. mori* silk in defected bone regeneration.[14] Recently, the electrospun SF nanofiber membrane has aroused great interest in GBR because its interconnected porous structure can prevent ingrowth of soft tissue and support the transport of metabolic nutrients and waste.[11] However, the time-consuming process, poor mechanical properties of electrospun SF nanofibers, and a toxic solvent limit the wide application of the electrospinning method for preparing SF GBR membranes. Therefore, it is necessary to develop an efficient and green method to prepare SF nanofibrous membranes with superior performance.

To achieve high performance, a hierarchically complex structure was assembled in native materials.[15] For example, silk consists of tens of thousands of nanofibers with a diameter of approximately 20 nm, which endows silk with ultrastrong properties.[16] Nanofibrous materials have great potential application in regenerative medicine because of their extracellular matrix (ECM)-mimetic structure. Recently, a facile versatile top-down method using physical shearing was reported to extract nanofibers directly from natural silk.[17] Compared with electrostatic spinning, the preparation of silk nanofibers by physical shearing does not require the use of toxic solvents, causes less damage to the protein molecular structure of SF, and is greener and safer, and the mechanical properties of the nanofibers are superior. In addition, it also has the advantages of large yield, low energy consumption, and short preparation time.[18,19]

In the present study, tussah silk nanofiber (TSn) and *B. mori* silk nanofiber (BSn) membranes were prepared using the high-speed shear method. The morphology, structure, and mechanical properties of the membranes were characterized. In vitro cell biocompatibility and osteogenic generation in rat cranial defect were studied on the TSn membrane and compared with the BSn membrane. The study is of great significance given the promising application of SF nanofibrous membranes in GBR.

2. MATERIALS AND METHODS

2.1. Materials. Tussah silk (Jiangsu, China), *B. mori* silk (Jiangsu, China), anhydrous sodium carbonate (Na_2CO_3, China National Pharmaceutical Group Corporation), anhydrous ethanol (China National Pharmaceutical Group Corporation), mouse embryonic osteogenic precursor cells (MC3T3-E1, BNCC), DMEM high-sugar medium (Gibco), fetal bovine serum (FBS, Procell), penicillin−streptomycin (Sigma), 0.25% trypsin digestive solution (Sigma), dimethyl sulfoxide (Sigma), paraformaldehyde (PFA) (Sigma), rhodamine−phalloidin (Sigma), Hoechst 33258 (Beijing Solarbio Technology Co., LTD.), Triton X-100 (Sigma), and a CCK-8 kit (Shanghai Beyotime Biotechnology Co., Ltd.) are the materials and instruments used in this study.

2.2. Preparation of Silk Nanofiber Membranes. Tussah silk was boiled in 0.5 wt % Na_2CO_3 solution for 0.5 h at a bath ratio of 1:50, repeated three times to remove sericin and then put into a 60 °C oven for drying. *B. mori* silk was degummed with 0.05 wt % Na_2CO_3 solution and dried after degumming through the same steps. The degummed tussah silk and *B. mori* silk were cut into 0.5 cm pieces, mixed with deionized water at a bath ratio of 1:100, and then put into a 32,000 rpm high-

speed blender with a four-blade blunt knife (Joyoung, Shandong, China) for 30 min to obtain tussah silk nanofiber slurry and *B. mori* silk nanofiber slurry. The concentration of silk nanofiber slurry was about 1 wt %, and 20 g slurry was poured into a Petri dish with a diameter of 9 mm and then dried in oven at 60 °C for about 4 h to obtain TSn and BSn.[17,20]

2.3. Characterization. The morphology of the TSn and BSn membranes was observed using a scanning electron microscope (8100, Hitachi, Tokyo, Japan) at 3 kV. SEM images of TSn and BSn were measured by ImageJ software to obtain the average diameter of the fibers. The secondary structure of the TSn and BSn membranes was determined by Fourier transform infrared spectroscopy (FTIR) in the range of 400−4000 cm^{-1}.

2.4. Mechanical Properties. The TSn and BSn membranes were cut into 50 mm × 10 mm rectangles. The thickness of the membrane was measured with a vernier caliper at five different positions of the membrane, and then the average value was taken. An Instron 5967 universal material testing machine (Boston, USA) was used to test the mechanical properties. Before the test, the sample was placed in a room with constant temperature and humidity (25 ± 0.5 °C; 60 ± 5% relative humidity) for 24 h. During the test, the instrument clamping distance was 30 mm, the tensile rate was 5 mm/min, and the pretension was 0.2 CN. The number of each sample was 5.

2.5. Biocompatibility. *2.5.1. Cell Culture and Proliferation.* The TSn and BSn membranes were cut into 5 mm discs, placed in 48-well plates after high temperature and pressure (121 °C and 200 kPa) sterilization for 30 min, and soaked in α-modified Eagle's medium (a-MEM, Gibco, USA). MC3T3-E1 was cultured in a-MEM supplemented with 10% FBS and 1% penicillin/streptomycin under standard conditions (37 °C, 5% CO_2, and 95% humidity) up to 80% confluency before passaging. The cells growing to the third generation were digested, and the concentration of the cell suspension was adjusted to 800 cells per microliter. 50 μL of cell suspension was inoculated on the membrane surface and incubated for 2 h to promote cell adhesion, and then, the cell culture medium was added. The culture medium was changed every 2 days. After 1, 3, and 7 days, the membrane with cells was moved into a new well for a CCK-8 test. The CCK-8 solution was added to each well and incubated for 2 h. After that, 100 μL of supernatant was removed from each well and added to a 96-well plate and then transferred to a microplate meter to test the absorbance value at 450 nm (OD).

2.5.2. Laser Confocal Microscopy Observation. The cell culture solution containing the sample was absorbed and placed in a waste liquid bottle after 1 d, 3 d, and 7 d of culture. The sample was washed gently with sterile PBS buffer at least 3 times. After that, the cells on the sample were fixed with 300 μL of 4% PFA solution for 30 min, which was treated with 500 μL of Triton X-100 solution for 15 min; the Triton X-100 solution was removed and the cells were gently washed with PBS buffer 3 times. The rhodamine−phalloidin solution was configured at a ratio of 1:800. Then, 500 μL of rhodamine solution was added and incubated for 40 min under dark conditions for staining. Rhodamine solution was desorbed and washed with PBS buffer 3 times for 5 min each time. Hoechst 33258 solution was prepared at a ratio of 1:1000, and 500 μL of Hoechst 33258 solution was added to avoid light and incubated for 15 min. The Hoechst 33258 solution was
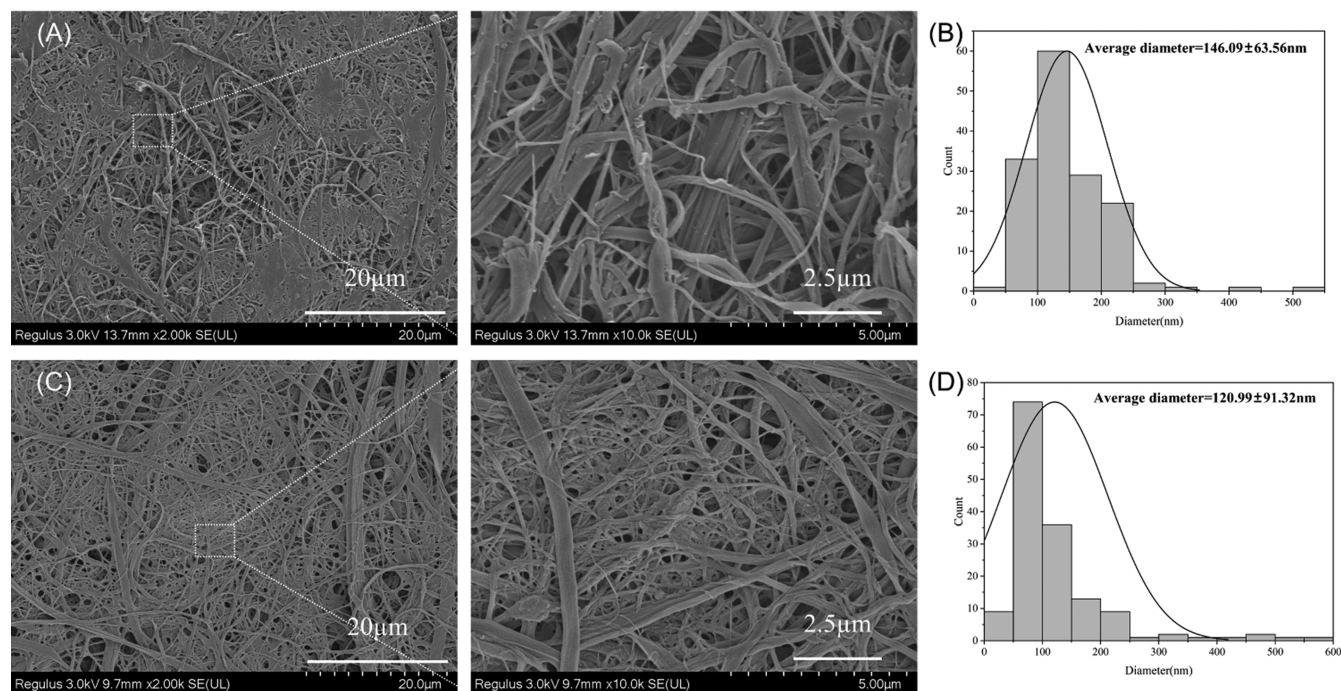
Figure 1. SEM images and diameter distribution of the silk nanofiber membrane. (A,B) TSn membrane and (C,D) BSn membrane.

desorbed and cleaned with PBS buffer 3 times. The cytoskeleton was observed under a laser confocal microscope, and the nucleus was blue.

2.6. In Vivo Study. *2.6.1. Surgical Procedure.* To evaluate the properties of membranes in vivo, 15 7−8 week-old male rats were used. All procedures in this study were performed in accordance with the Animal Care and Experiment Committee of Institute of Soochow University (Suzhou, China). Fifteen healthy male Sprague-Dawley rats with an average body weight of 250 g (≈7−8 weeks) were used in this study. The rats were randomly divided into three groups: (1) TSn; (2) BSn; and (3) control. The rats were given general anesthesia by intraperitoneal injection of 4% chloral hydrate (1 mL/100 g body weight). Once completely anesthetized, the animals were positioned on the operating table in a prone position. The cranium was exposed through a midline skin incision. The surgical site was carefully shaved and disinfected with povidone iodine, and a longitudinal incision was made along the midline in the skull from the nasal to the occipital region. After separating the full-thickness skin and skin-periosteal muscle, the cranial surface on both sides of the midline was exposed. Five millimeter-diameter bilateral full-thickness cranial defects were made in the bones using a standardized dental-trephine bur under copious sterile saline irrigation. Two 5 mm-diameter defects were created, one on each side of the midline.

During the punching process, extreme care was taken to avoid perforation of the dura mater. After removal of the trephined cranial bone. Then, cranial defects were covered with TSn and BSn membranes on the bone surface (test group). No membranes were placed in the control group defects (control group). Later, all membranes were trimmed into rectangles (14 mm × 7 mm in size) to fit the defects well. The pericranium and skin were sutured in layers with 3−0 silk sutures. After surgery, the rats were caged and received food and water individually. Five animals were used in every group. The rats were sacrificed at 4 and 12 weeks. Then, the cranial samples, including both the defects, the membranes, and the surrounding tissue, were removed from the bodies. These samples were fixed with 4% PFA for 24 h at room temperature.

2.6.2. Microcomputed Tomography Analysis. The prepared samples were scanned by microcomputed tomography (CT) (SkyScan 1176; Bruker-microCT, Kontich, Belgium). The scanning conditions were set at a voltage of 65 kV, current of 100 μA, 600 ms exposure time, and Al filter of 1 mm. The width of scanning was 50 mm, and the radiator axis was perpendicular to the surface of the bone defect. The system software was used to reconstruct three-dimensional images. The upper and lower threshold values for bone were 255 and 75 gray, respectively. The images were reconstructed from the axial, sagittal, and coronal planes. Since the initial bone defect was round with a diameter of 5 mm, the region of interest (ROI) was selected to reflect the initial shape. Bone volume (BV) and tissue volume (TV) analyses were performed for the ROI in each sample. Four samples at 4 weeks and six samples at 12 weeks were taken for micro-CT.

2.6.3. Histological Staining. Following micro-CT testing, samples were decalcified in 10% ethylenediaminetetraacetic acid for 2−4 weeks and dehydrated in a fractional series of ethanol. Then, samples were embedded in paraffin wax and cut into 5 μm sections from the center area of the bone defects. For histological staining, the sections were stained with hematoxylin and eosin (H&E) and Masson's trichrome staining and then evaluated using a microscope (Axioveter 40 CFL, Zeiss, Germany). Four samples at 4 weeks and six samples at 12 weeks were taken for histological analysis.

2.7. Statistical Analysis. All quantitative data are presented as the mean ± standard deviation. The *t*-test and one-way analysis of variance were performed to assess the statistical significance of the results, and $p < 0.05$ was considered to be significant.

3. RESULTS AND DISCUSSION

3.1. Morphology Observation. Figure 1 shows the TSn and BSn membranes derived from native tussah and *B. mori* silk. The surface of the two membranes was a network structure formed by random interlacing of nanofibers. The surface and interior of the TSn membrane were more compact than those of the BSn membrane, which showed a rougher surface. Although $Ca(NO_3)_2/CH_3CH_2OH/H_2O$ solution treatment had been used to assist nanofiber exfoliation,[20] it was not a necessary step to obtain silk nanofibers. In this study, the degummed silk was directly used to fabricate nanofiber membranes by physical shearing, avoiding the time-consuming process and potential solvent residual. The thicknesses of TSn and BSn were about 0.21 and 0.19 mm, respectively, and the corresponding average diameters were 146.09 ± 63.56 and 120.99 ± 91.32 nm, respectively. Note that the diameter of BSn obtained in this study was smaller than that derived from $Ca(NO_3)_2/CH_3CH_2OH/H_2O$-treated silk reported previously.[20] After high-speed shear treatment, the original structure of silk was disrupted to form silk nanofibers through destroying the interaction forces between nanofibrils.[21,22] The membrane formed by the nanofibers had a large specific surface area, which made the cells have a larger contact area when growing on the membrane surface.[22] Meanwhile, the nanoscale fiber was similar to the nanofibrous structure of the ECM, which was conducive to cell adhesion, migration, and proliferation.[23]

3.2. Structure Analysis. The secondary structure of the TSn and BSn membranes was determined by using FTIR, as shown in Figure 2. The TSn membrane showed absorption
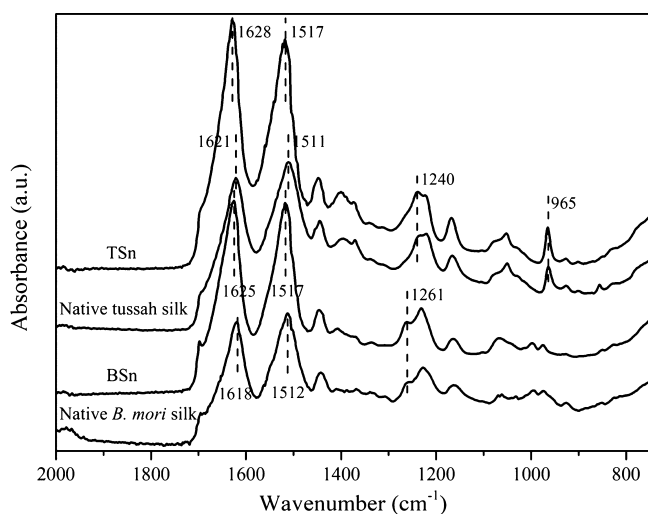

Figure 2. FTIR spectra of TSn and BSn membranes.

peaks at 1628 cm^{-1} (amide I), 1517 cm^{-1} (amide II), 1240 cm^{-1} (amide III), and 965 cm^{-1} (amide IV), corresponding to the β-sheet structure.[24−26] The BSn membrane exhibited absorption peaks at 1625 cm^{-1} (amide I), 1517 cm^{-1} (amide II), and 1261 cm^{-1} (amide III), which were also ascribed to the β-sheet structure.[25,27] The processing of TSn and BSn membranes was a physical method that only destroyed the interfacial forces of the nanofibers. It can be observed in Figure 2 that the IR spectra of TSn and BSn were similar to those of native tussah silk and *B. mori* silk. Therefore, the β-sheet structure in native silk was mainly retained in the resulting silk nanofiber membrane. The main β-sheet structure endowed the

silk nanofiber membrane with structural stability and good mechanical properties.[26]

3.3. Mechanical Properties. The mechanical properties of the TSn and BSn membranes were measured, as shown in Figure 3. Young's modulus, stress, and strain of the BSn membrane were 0.16 ± 0.03 GPa, 4.86 ± 0.61 MPa, and 6.24 ± 0.41%, respectively. Compared with the BSn membrane, the TSn membrane showed superior mechanical properties. Young's modulus, stress, and strain of the TSn membrane were 3.61 ± 0.64 GPa, 74.27 ± 5.19 MPa, and 2.51 ± 0.24%, which were significantly higher than those of silk GBR films prepared by electrospinning.[1−3,28] As can be seen from Figure 1, the structure of TSn was relatively loose and the fiber was stretched, while the structure of BSn was relatively compact and the fiber was curved. During stretching, most fibers in TSn resisted the external force together, while only partial fibers in BSn bear stretching due to the curved state of the fibers. In addition, the breaking stress and toughness of native tussah silk was significantly higher than that of native *B. mori* silk.[22] The superior mechanical properties of native tussah silk and the different fiber state of SF nanofibers made the strength and Young's modulus of TSn higher than that of BSn. The fracture of the nanofiber membrane was mainly dominated by nanofiber fracture and pull-out.[29] TSn was easier to pull out under stretching than BSn due to its looser structure (Figure 1), resulting in a low friction effect. The strain-to-failure was significantly decreased in TSn due to its weak interfiber interaction, and it increased in BSn because of its interlaced nanofiber structure. Therefore, compared with BSn, TSn showed higher breaking strength and lower strain in the tensile test. It was reported that the stresses of the electrospun silk nanofiber membrane and collagen membrane were about 9[28] and 27 MPa,[5] which were lower than that of the TSn membrane. The excellent mechanical properties of the silk nanofiber membrane, especially the TSn membrane, could provide effective protection for bone defects, thus allowing the ingrowth of new bone.[18]

3.4. Biocompatibility. The morphologies of MC3T3-E1 cells grown on TSn and BSn membranes at 1, 3, and 7 days were observed using a laser confocal microscope, as shown in Figure 4A. The cells displayed a spindle shape, and the number of cells on the nanofiber membranes increased gradually with time. Figure 4B shows that the numbers of cells that grew on TSn and BSn membranes increased gradually with increasing culture time. It was noted that the cell numbers grown on the TSn membrane were significantly higher than those grown on the BSn membrane at 3 and 7 d.

Although SF is biocompatible and biodegradable, the lack of a bioactive domain limits its therapeutic efficacy.[30] RGD is a highly effective cell recognition sequence to modulate cell−material interactions, such as cell adhesion, migration, angiogenesis, and differentiation.[13] Cell adhesion and proliferation are crucial for biomaterials in repairing damaged tissue. Attempts have been made to incorporate the RGD sequence in the *B. mori* SF scaffold to improve its bioactivity.[13,31] The SF scaffold derived from tussah silk contains a natural RGD sequence, which has been found to significantly promote cell adhesion, osteogenic differentiation, and mineralization.[32] In this study, tussah silk was disintegrated into nanofibers by physical shearing, and then these silk nanofibers were processed into membranes by air drying. The silk nanofiber membrane, mimicking the structure of the ECM, was conducive to cell adhesion, proliferation, and migration.[33]
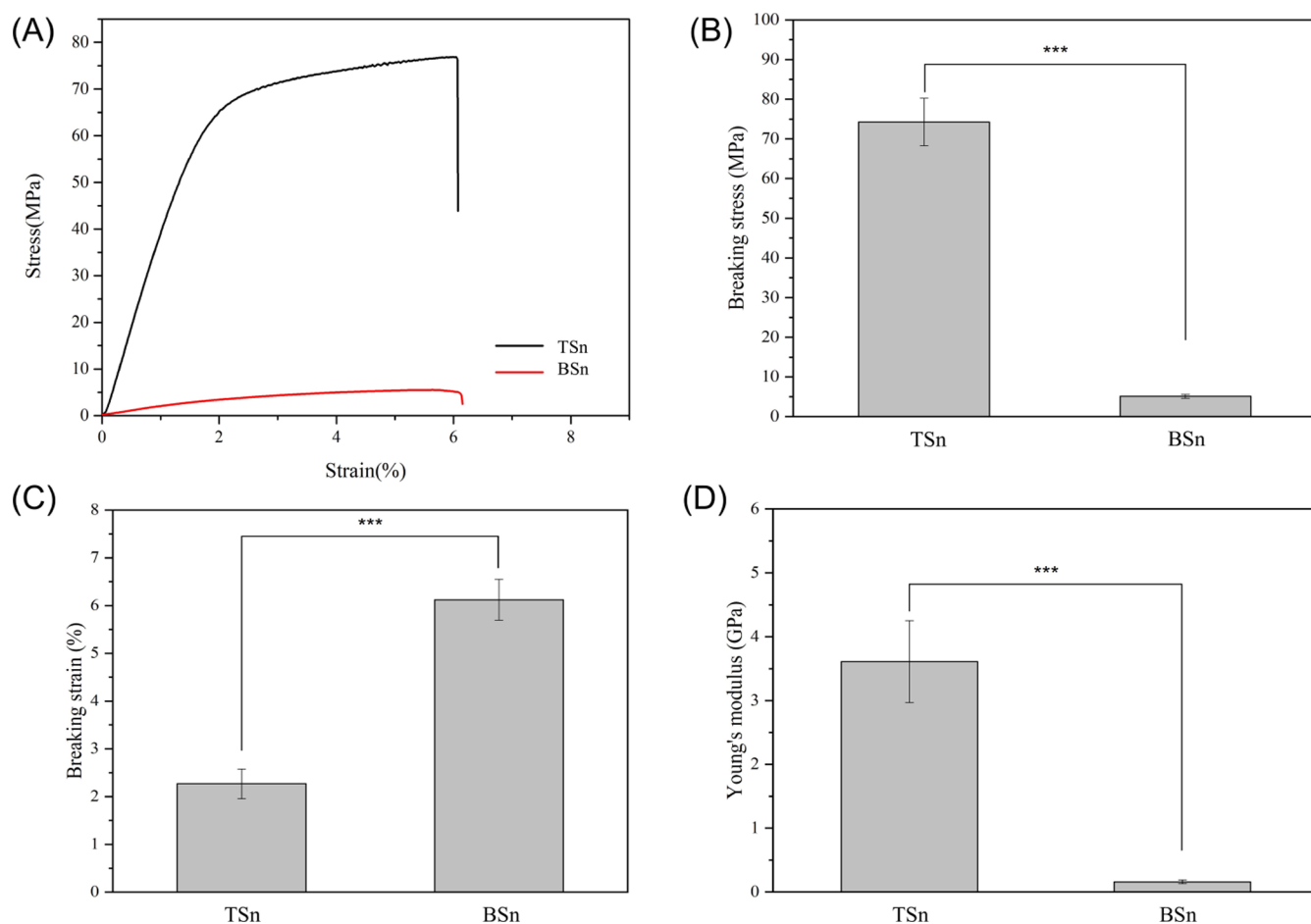
Figure 3. Mechanical properties of TSn and BSn membranes. (A) Strain−stress curves, (B) breaking stress, (C) breaking strain, and (D) Young's modulus (***$p < 0.001$, $n = 5$).
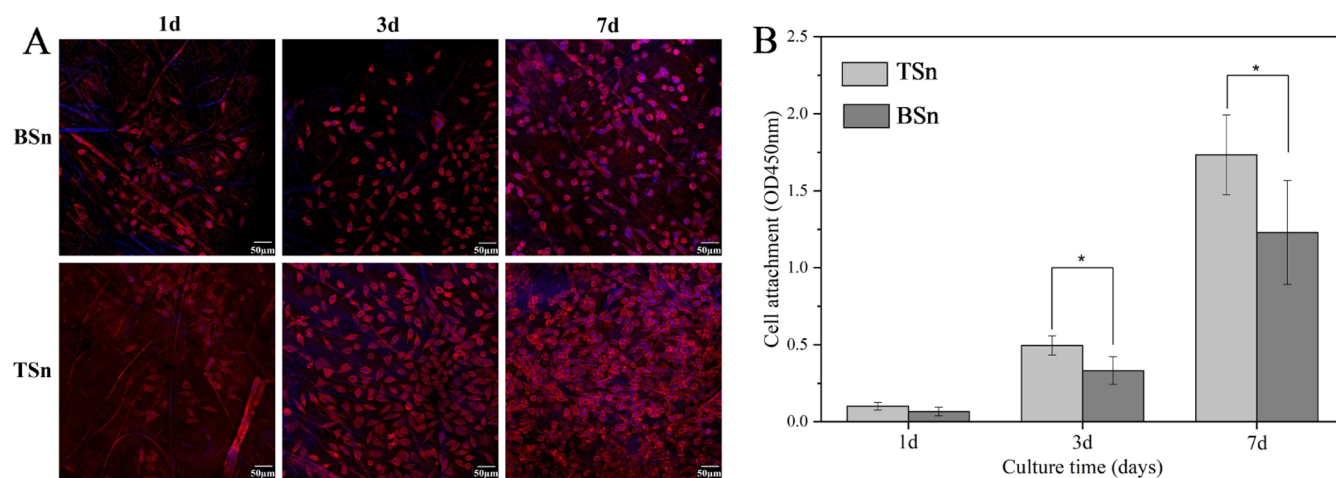

Figure 4. Laser confocal images (A) and CCK-8 TEST of the proliferation activity (B) of MC3T3-E1 cells grown on TSn and BSn membranes (*$p < 0.05$, $n = 5$).

In addition, TSn contained an RGD tripeptide sequence, which was a cell adhesion recognition signal. Therefore, the TSn membrane displayed an intrinsic propensity to improve cell adhesion and proliferation compared with the BSn membrane.[14]

3.5. Micro-CT Analysis. We prepared a rat cranial bone defect model to investigate the bone regeneration capacity of silk nanofiber membranes. After surgery, all rats regained

consciousness and remained healthy until the end of the study, and no significant weight loss, membrane rejection, or other postoperative infections happened. The micro-CT images are shown in Figure 5A. Overall, the bone formation increased gradually from 4 to 12 weeks, suggesting the intrinsic regeneration capacity of native bone. Negligible new bone formation was observed in the inner edge of the control group without membrane cover mostly due to the ingrowth of the
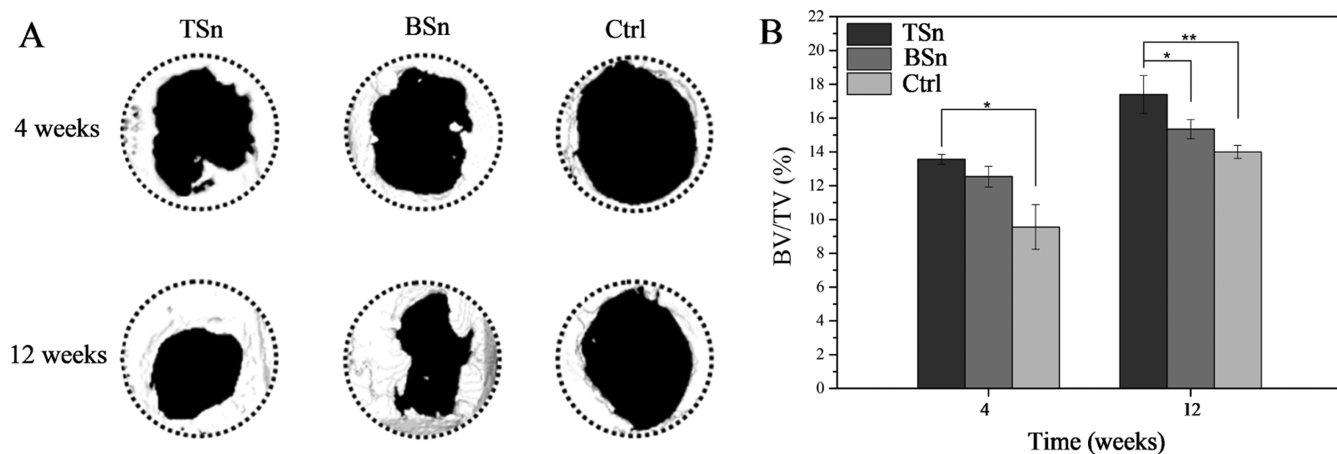
Figure 5. Micro-CT analysis of bone reconstruction in a calvarial defect model of rat using silk nanofiber membranes. (A) μCT images and (B) BV/TV ratio (*$p < 0.05$, **$p < 0.01$, $n = 3$).

surrounding soft tissue.[34] Compared to the control group, the bone area newly formed was significantly bigger in the silk nanofiber membrane group, achieving the best bone reconstruction in the TSn group.

The quantitative analysis from μCT images for regenerated bone is shown in Figure 5B. The BV/TV ratio increased gradually in all groups and showed a significant difference among the three groups. The BV/TV values 12 weeks after operation were 17.40 ± 1.11, 15.35 ± 0.57, and $13.99 \pm 0.38\%$ in the TSn, BSn, and control groups, respectively. The best bone reconstruction was achieved for TSn, followed by BSn and then the control group. The silk nanofiber membrane achieved better results than the control group because of the barrier membranes preventing soft tissue invasion and facilitating new bone regeneration.[34] In addition, TSn showed higher bone regeneration compared to BSn. It was believed that the different osteogenesis was attributed to the presence of an RGD sequence in TSn and a lack in BSn. The RGD sequence was known to promote the adhesion and spreading of osteoblasts and colony formation.[13] In addition, the combination of $\alpha5\beta1$ integrin and RGD present in TSn could activate the BMP-2 signaling pathway.[14] The improved cell adhesion, proliferation and colony formation, and activated BMP-2 signaling pathway may contribute to the enhanced bone regeneration in vivo.[14,35]
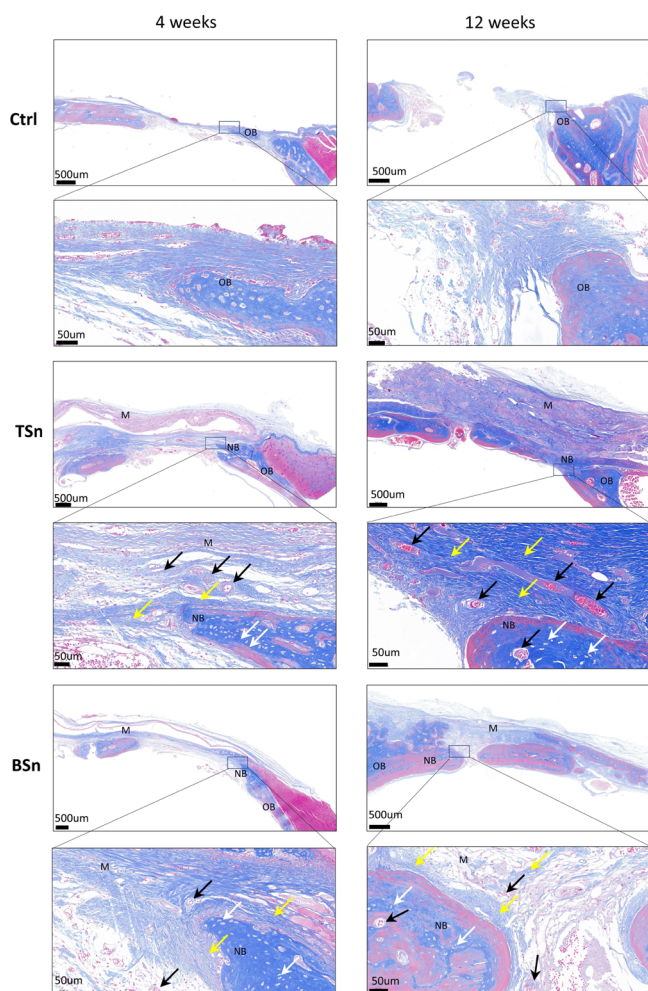
3.6. Histological Analysis. In order to validate the μCT observation, histological studies were conducted. The results of H&E and Masson's trichrome staining at 4 and 12 weeks are shown in Figures 6 and 7. The control group without membranes was invaded by thin, loosely organized connective tissues. Only a limited amount of bone regeneration was observed in the defect rim at both 4 and 12 weeks. In contrast, a visible new bone regeneration at 4 weeks and nearly a bone bridge crossed the defect areas formed at 12 weeks for both BSn and TSn groups. However, some inflammatory cells (including neutrophils, lymphocytes, and macrophages) were observed at the defect boundary of the SF groups. The immune response and adverse reaction of the biomaterial after in vivo implantation are important. Despite local inflammation, a new bone tissue was formed under the guidance of BSn and TSn, suggesting that the immune response of the SF was acceptable.[36] In TSn and BSn groups, abundant blood vessels formed near the new bone (Figures 6 and 7, black arrows). In addition, many osteoblasts appearing around and inside the
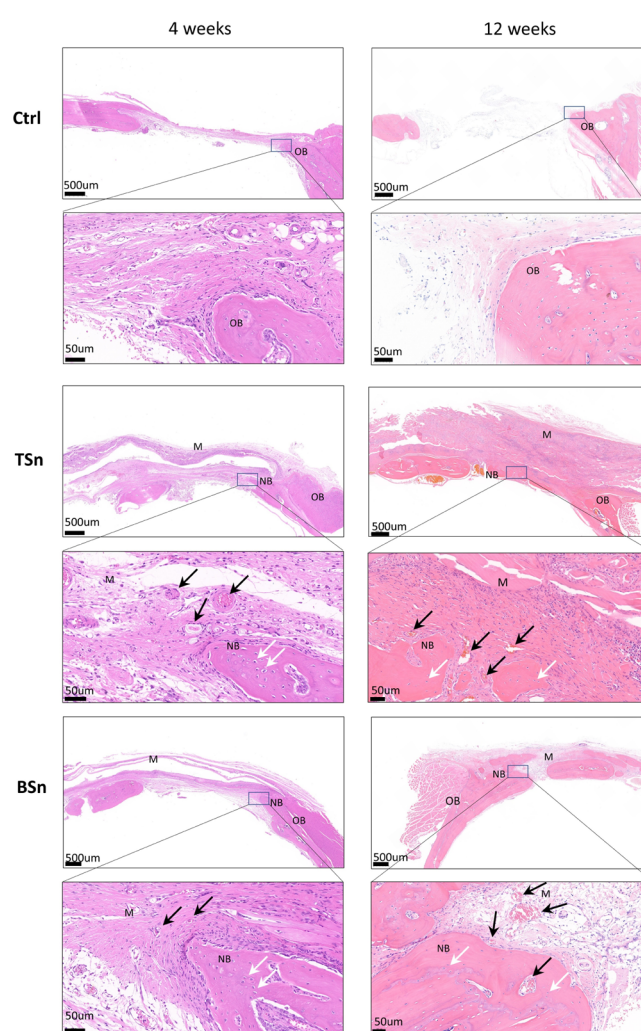
Figure 6. Histological observation with HE staining of control and TSn and BSn membrane groups at 4 and 12 weeks after surgery. M: nanofiber membrane, NB: new bone, OB: old bone. Black arrows indicate blood vessels and white arrows indicate osteoblasts.

new bone was observed (Figures 6 and 7, white arrows). Meanwhile, numerous fiber-like structures (Figure 7, yellow arrows) surrounded the new bone, suggesting typical collagen

Figure 7. Histological observation with Masson trichromatic staining of control and TSn and BSn membrane groups at 4 and 12 weeks after surgery. M: nanofiber membrane, NB: new bone, OB: old bone. Black arrows indicate blood vessels; white arrows indicate osteoblasts; yellow arrows indicate collagen fibers.

a result, the osteogenic tissue formation was significantly promoted and guided by the biomimetic, biocompatible, high-strength, and highly stable TSn membrane.

GBR has become the standard procedure for periodontal regeneration threatment.[23] From an immunological point of view, SF is consistent with a good clinical experience. More importantly, SF materials are widely used in clinical research and application.[41] Many studies by us and other groups have assumed that SF materials are proper materials for application in GBR.[11] In the present study, the TSn group exhibited superior osteoconductivity compared to that of the BSn group. Therefore, the excellent biocompatibility, biomimetic nanofibrous structure, and good mechanical properties made TSn a promising material for application in GBR.

4. CONCLUSIONS

In summary, natural TSn and BSn membranes were developed and compared for efficacious bone tissue regeneration. TSn and BSn showed a network structure with interwoven nanofibers, and the fiber diameters were 146.09 ± 63.56 and 120.99 ± 91.32 nm, respectively. TSn showed a higher tensile strength and a modulus of 74.27 ± 5.19 MPa and 3.61 ± 0.64 GPa, which were superior to those of BSn and electrospun SF nanofiber membranes reported previously. In vitro studies demonstrated that enhanced cell adhesion and proliferation was achieved on TSn compared to that on BSn. Consistent with the in vitro results, TSn promoted bone regeneration in rat skull defect model. The aqueous-derived TSn has inherently RGD sequence, nanofibrous structure, and excellent mechanical properties, which is suitable for bone tissue repair. Further study is warranted to evaluate the degradation of TSn and tune it to match bone regeneration, making it a more promising membrane of GBR.

■ AUTHOR INFORMATION

Corresponding Authors

Shijun Lu − *Suzhou Stomatological Hospital, Suzhou Medical College of Soochow University, Suzhou 215005, China; Jiangsu Key Laboratory of Oral Diseases, Nanjing Medical University, Nanjing 210029, China;* Email: lu.sj@foxmail.com

Minxuan Han − *Jiangsu Key Laboratory of Oral Diseases, Nanjing Medical University, Nanjing 210029, China; Department of Orthodontics, Affiliated Hospital of Stomatology, Nanjing Medical University, Nanjing 210029, China;* Email: 178031043@qq.com

Authors

Yumao Chen − *Suzhou Stomatological Hospital, Suzhou Medical College of Soochow University, Suzhou 215005, China;* orcid.org/0000-0002-1970-2921

Ming Chen − *National Engineering Laboratory for Modern Silk, College of Textile and Clothing Engineering, Soochow University, Suzhou 215123, China*

Yang Gao − *Department of Stomatology, The First Affiliated Hospital of Soochow University, Suzhou 215005, China*

Feng Zhang − *National Engineering Laboratory for Modern Silk, College of Textile and Clothing Engineering, Soochow University, Suzhou 215123, China;* orcid.org/0000-0001-6348-5816

Min Jin − *Suzhou Stomatological Hospital, Suzhou Medical College of Soochow University, Suzhou 215005, China*

Complete contact information is available at:

deposition, which served as nucleation sites for bone mineralization.[37]

Many studies have demonstrated that the SF membrane is suitable for GBR.[1,11,23,38] The SF membrane can provide mechanical stability and structural integrity to prevent tissue invasion and to retain space for bone regeneration.[23,38] In the present study, BSn and TSn membranes all appeared intact under the microscope (Figures 6 and 7), showing few signs of resorption or distortion after 12 weeks of operation. The degradation time for regenerated SF scaffolds in vivo was more than 1 year,[39] while the natural silk fiber, especially nonmulberry silk, presented a longer degradation period.[40] Therefore, the BSn and TSn membranes retained in the bone defect could be responsible for the less soft and more bone tissue ingrowth. A large number of blood vessels around the new bone were observed, which could provide enough nutrition for bone formation. Collagen fibers are the central component in the natural bone matrix.[37] The abundance of collagen fibers was found near the new bone (Figure 7), which could act as a template for further formation of hydroxyapatite. In addition, tussah silk exhibits superior osteoconductivity than *B. mori* silk, including cell proliferation and osteoblast differentiation in vitro[32] and bone regeneration in vivo.[14] As

https://pubs.acs.org/10.1021/acsomega.2c01784

■ REFERENCES

(1) Cai, Y.; Guo, J.; Chen, C.; Yao, C.; Chung, S.-M.; Yao, J.; Lee, I.-S.; Kong, X. Silk fibroin membrane used for guided bone tissue regeneration. *Mater. Sci. Eng., C* 2017, 70, 148−154.

(2) Kwon, K.-J.; Seok, H. Silk Protein-Based Membrane for Guided Bone Regeneration. *Appl. Sci.* 2018, 8, 1214.

(3) Türkkan, S.; Pazarçeviren, A. E.; Keskin, D.; Machin, N. E.; Duygulu, Ö.; Tezcaner, A. Nanosized CaP-silk fibroin-PCL-PEG-PCL/PCL based bilayer membranes for guided bone regeneration. *Mater. Sci. Eng., C* 2017, 80, 484−493.

(4) Zhao, Y.; Chen, J.; Chou, A. H. K.; Li, G.; LeGeros, R. Z. Nonwoven silk fibroin net/nano-hydroxyapatite scaffold: Preparation and characterization. *J. Biomed. Mater. Res., Part A* 2009, 91, 1140−1149.

(5) Lee, S.-W.; Kim, S.-G. Membranes for the Guided Bone Regeneration. *Maxillofac. Plast. Reconstr. Surg.* 2014, 36, 239−246.

(6) Jung, R. E.; Fenner, N.; Hämmerle, C. H. F.; Zitzmann, N. U. Long-term outcome of implants placed with guided bone regeneration (GBR) using resorbable and non-resorbable membranes after 12-14 years. *Clin. Oral Implants Res.* 2013, 24, 1065−1073.

(7) Lorenzoni, M.; Pertl, C.; Polansky, R. A.; Jakse, N.; Wegscheider, W. A. Evaluation of implants placed with barrier membranes. *Clin. Oral Implants Res.* 2002, 13, 274−280.

(8) Guo, H.; Xia, D.; Zheng, Y.; Zhu, Y.; Liu, Y.; Zhou, Y. A pure zinc membrane with degradability and osteogenesis promotion for guided bone regeneration: In vitro and in vivo studies. *Acta Biomater.* 2020, 106, 396−409.

(9) Bottino, M. C.; Thomas, V.; Schmidt, G.; Vohra, Y. K.; Chu, T.-M. G.; Kowolik, M. J.; Janowski, G. M. Recent advances in the development of GTR/GBR membranes for periodontal regeneration-A materials perspective. *Dent. Mater.* 2012, 28, 703−721.

(10) Melke, J.; Midha, S.; Ghosh, S.; Ito, K.; Hofmann, S. Silk fibroin as biomaterial for bone tissue engineering. *Acta Biomater.* 2016, 31, 1−16.

(11) Lu, S.; Wang, P.; Zhang, F.; Zhou, X.; Zuo, B.; You, X.; Gao, Y.; Liu, H.; Tang, H. A novel silk fibroin nanofibrous membrane for guided bone regeneration: a study in rat calvarial defects. *Am. J. Transl. Res.* 2015, 7, 2244−2253.

(12) Santin, M.; Motta, A.; Freddi, G.; Cannas, M. In vitro evaluation of the inflammatory potential of the silk fibroin. *J. Biomed. Mater. Res.* 1999, 46, 382−389.

(13) Xu, F.; Liu, J.; Tian, J.; Gao, L.; Cheng, X.; Pan, Y.; Sun, Z.; Li, X. Supramolecular Self-Assemblies with Nanoscale RGD Clusters Promote Cell Growth and Intracellular Drug Delivery. *ACS Appl. Mater. Interfaces* 2016, 8, 29906−29914.

(14) Sahu, N.; Baligar, P.; Midha, S.; Kundu, B.; Bhattacharjee, M.; Mukherjee, S.; Mukherjee, S.; Maushart, F.; Das, S.; Loparic, M.; et al. Nonmulberry Silk Fibroin Scaffold Shows Superior Osteoconductivity Than Mulberry Silk Fibroin in Calvarial Bone Regeneration. *Adv. Healthcare Mater.* 2015, 4, 1709−1721.

(15) Zhao, H.-P.; Feng, X.-Q.; Gao, H. Ultrasonic technique for extracting nanofibers from nature materials. *Appl. Phys. Lett.* 2007, 90, 073112.

(16) Du, N.; Yang, Z.; Liu, X. Y.; Li, Y.; Xu, H. Y. Structural Origin of the Strain-Hardening of Spider Silk. *Adv. Funct. Mater.* 2011, 21, 772−778.

(17) Li, L.; Yang, H.; Li, X. F.; Yan, S. Q.; Xu, A. C.; You, R. C.; Zhang, Q. Natural silk nanofibrils as reinforcements for the preparation of chitosan-based bionanocomposites. *Carbohydr. Polym.* 2021, 253, 117214.

(18) Li, X.; Zhang, Q.; Ye, D.; Zhang, J.; Guo, Y.; You, R.; Yan, S.; Li, M.; Qu, J. Fabrication and characterization of electrospun PCL/Antheraea pernyisilk fibroin nanofibrous scaffolds. *Polym. Eng. Sci.* 2017, 57, 206−213.

(19) Ang, S. L.; Shaharuddin, B.; Chuah, J.-A.; Sudesh, K. Electrospun poly(3-hydroxybutyrate-co-3-hydroxyhexanoate)/silk fibroin film is a promising scaffold for bone tissue engineering. *Int. J. Biol. Macromol.* 2020, 145, 173−188.

(20) Cai, J.; Wang, Q.; Li, X.; Guan, Y.; He, L.; Yan, S.; You, R.; Zhang, Q. Water-stable natural silk nanofibril composite films for electrical devices. *Mater. Today Commun.* 2020, 22, 100776.

(21) Fang, G.; Tang, Y.; Qi, Z.; Yao, J.; Shao, Z.; Chen, X. Precise correlation of macroscopic mechanical properties and microscopic structures of animal silks-using Antheraea pernyi silkworm silk as an example. *J. Mater. Chem. B* 2017, 5, 6042−6048.

(22) Fu, C.; Porter, D.; Chen, X.; Vollrath, F.; Shao, Z. Understanding the Mechanical Properties ofAntheraea PernyiSilk-From Primary Structure to Condensed Structure of the Protein. *Adv. Funct. Mater.* 2011, 21, 729−737.

(23) Kim, K.-H.; Jeong, L.; Park, H.-N.; Shin, S.-Y.; Park, W.-H.; Lee, S.-C.; Kim, T.-I.; Park, Y.-J.; Seol, Y.-J.; Lee, Y.-M.; et al. Biological efficacy of silk fibroin nanofiber membranes for guided bone regeneration. *J. Biotechnol.* 2005, 120, 327−339.

(24) Kweon, H.; Park, Y. H. Dissolution and characterization of regeneratedAntheraea pernyi silk fibroin. *J. Appl. Polym. Sci.* 2001, 82, 750−758.

(25) Tao, W.; Li, M.; Zhao, C. Structure and properties of regenerated Antheraea pernyi silk fibroin in aqueous solution. *Int. J. Biol. Macromol.* 2007, 40, 472−478.

(26) Callone, E.; Dirè, S.; Hu, X.; Motta, A. Processing Influence on Molecular Assembling and Structural Conformations in Silk Fibroin: Elucidation by Solid-State NMR. *ACS Biomater. Sci. Eng.* 2016, 2, 758−767.

(27) Narita, C.; Okahisa, Y.; Wataoka, I.; Yamada, K. Characterization of Ground Silk Fibroin through Comparison of Nanofibroin and Higher Order Structures. *ACS Omega* 2020, 5, 22786−22792.

(28) Zhang, F.; Lu, Q.; Ming, J.; Dou, H.; Liu, Z.; Zuo, B.; Qin, M.; Li, F.; Kaplan, D. L.; Zhang, X. Silk dissolution and regeneration at the nanofibril scale. *J. Mater. Chem. B* 2014, 2, 3879−3885.

(29) Benítez, A. J.; Torres-Rendon, J.; Poutanen, M.; Walther, A. Humidity and Multiscale Structure Govern Mechanical Properties and Deformation Modes in Films of Native Cellulose Nanofibrils. *Biomacromolecules* 2013, 14, 4497−4506.

(30) Chen, Z.; Zhang, Q.; Li, H.; Wei, Q.; Zhao, X.; Chen, F. Elastin-like polypeptide modified silk fibroin porous scaffold promotes osteochondral repair. *Bioact. Mater.* 2021, 6, 589−601.

(31) Yan, Y.; Cheng, B.; Chen, K.; Cui, W.; Qi, J.; Li, X.; Deng, L. Enhanced Osteogenesis of Bone Marrow-Derived Mesenchymal Stem Cells by a Functionalized Silk Fibroin Hydrogel for Bone Defect Repair. *Adv. Healthcare Mater.* 2019, 8, 1801043.

(32) Mandal, B. B.; Kundu, S. C. Non-mulberry silk gland fibroin protein 3-D scaffold for enhanced differentiation of human mesenchymal stem cells into osteocytes. *Acta Biomater.* 2009, 5, 2579−2590.

(33) Wang, J.; Chen, Y.; Zhou, G.; Chen, Y.; Mao, C.; Yang, M. Polydopamine-Coated Antheraea pernyi (A. pernyi) Silk Fibroin Films Promote Cell Adhesion and Wound Healing in Skin Tissue Repair. *ACS Appl. Mater. Interfaces* 2019, 11, 34736−34743.

(34) Kim, B. N.; Ko, Y.-G.; Yeo, T.; Kim, E. J.; Kwon, O. K.; Kwon, O. H. Guided Regeneration of Rabbit Calvarial Defects Using Silk Fibroin Nanofiber-Poly(glycolic acid) Hybrid Scaffolds. *ACS Biomater. Sci. Eng.* **2019**, *5*, 5266−5272.

(35) Braccini, A.; Wendt, D.; Farhadi, J.; Schaeren, S.; Heberer, M.; Martin, I. The osteogenicity of implanted engineered bone constructs is related to the density of clonogenic bone marrow stromal cells. *J. Tissue Eng. Regener. Med.* **2007**, *1*, 60−65.

(36) Thurber, A. E.; Omenetto, F. G.; Kaplan, D. L. In vivo bioresponses to silk proteins. *Biomaterials* **2015**, *71*, 145−157.

(37) Ding, Z.; Cheng, W.; Mia, M.; Lu, Q. Silk Biomaterials for Bone Tissue Engineering. *Macromol Biosci* **2021**, *21*, 2100153.

(38) Seok, H.; Kim, M. K.; Kim, S.-G.; Kweon, H. Comparison of silkworm-cocoon-derived silk membranes of two different thicknesses for guided bone regeneration. *J. Craniofac. Surg.* **2014**, *25*, 2066−2069.

(39) Wang, Y.; Rudym, D. D.; Walsh, A.; Abrahamsen, L.; Kim, H.-J.; Kim, H. S.; Kirker-Head, C.; Kaplan, D. L. In vivo degradation of three-dimensional silk fibroin scaffolds. *Biomaterials* **2008**, *29*, 3415−3428.

(40) Zhao, C.; Wu, X.; Zhang, Q.; Yan, S.; Li, M. Enzymatic degradation of Antheraea pernyi silk fibroin 3D scaffolds and fibers. *Int. J. Biol. Macromol.* **2011**, *48*, 249−255.

(41) Chouhan, D.; Mandal, B. B. Silk biomaterials in wound healing and skin regeneration therapeutics: From bench to bedside. *Acta Biomater.* **2020**, *103*, 24−51.